AIAA SciTech Forum
January 3-7, 2022, San Diego, CA & Virtual
AIAA SCITECH 2022 Forum

10.2514/6.2022-0407

Propagating Instabilities in Coilable Booms

Wen Luo* and Sergio Pellegrino†
California Institute of Technology, Pasadena, CA, 91125, USA

Coilable booms consisting of thin composite shells bonded along a common edge are being considered for novel deployable spacecraft structures. These booms have many desirable features such as light weight, high stiffness, and high packaging efficiency, but this successful realization poses new challenges. In this paper, we study the propagating buckles that have been observed in the transition region between the coiled and deployed parts of the booms. These buckles, which can cause local stress concentrations and material failure, are typical of booms with built-up sections. They do not occur in tape springs. We investigate the root cause for the propagating buckles and discuss the possibility of limiting the buckle growth by increasing the material shear modulus.

Nomenclature

r	=	radius of the coiling hub
t	=	thickness of boom flange
w	=	width of boom web
R	=	radius of flange
ϕ	=	rotation of the coiling hub
θ_f	=	subtending angle of boom flange
γ	=	effective shear angle of the shear-lag region
ε_{ij}	=	in-plane strains at the mid-surface of inner flange
κ_{ij}	=	curvatures
F	=	reaction force at the loading point of buckling simulation
δ	=	edge shortening at the loading point of buckling simulation

I. Introduction

THE advent of ultra-thin laminated composite materials is driving the development of a new generation of large lightweight space structures as well as their packaging and deploying mechanisms. A commonly used structural element is the coilable boom, a cylindrical shell that can be elastically flattened and coiled on a hub. Examples include the basic tape spring, the STEM, the CTM [1] and, more recently, the Triangular Rollable And Collapsible (TRAC) boom [2]. These structures are coiled around a hub for launch and are deployed in space.

The detailed mechanics of these structures, which appear simple at first but in reality hide complex behaviors and pose several challenges in terms of structural stability, have been studied in several publications [3–5]. Recently, a particular kind of instability has been identified that is typical of built-up shells, i.e. consisting of at least two tape springs bonded along a common edge [6]. The study of this instability is the focus of the present paper.

Specifically, we study a TRAC boom with the cross-section shown in Fig. 1. The bonded region between the two shells is called the web, and the unbonded branches are called the flanges. The region where flanges are locally flattened but not yet coiled onto the hub is called the transition region. Reference [6, 7] studied the coiling of this structure and noticed the appearance of a buckle ahead of the coiled region, in the transition region marked in Fig. 2. The buckle occurs in the inner flange transition region and can be seen in Fig. 3. As noted in [7], local material damage, such as delamination and fiber kinking can occur when coiling tightly.

This phenomenon has recently been investigated [6] through a parametric study of the effect of the “flange length" (which is called “flange width" in the current study) on the size and shape of the buckle. Both finite element modeling

*Postdoctoral Researcher, Graduate Aerospace Laboratories, 1200 E California Blvd, Pasadena. wen-luo@caltech.edu AIAA Member.
†Joyce and Kent Kresa Professor of Aerospace and Civil Engineering, Graduate Aerospace Laboratories, 1200 E California Blvd. MC 105-50, Pasadena. sergiop@caltech.edu AIAA Fellow.

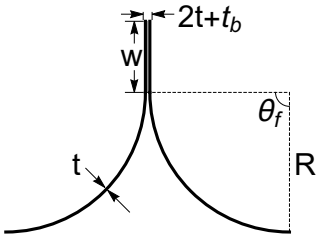

Fig. 1 Cross-section of TRAC boom.

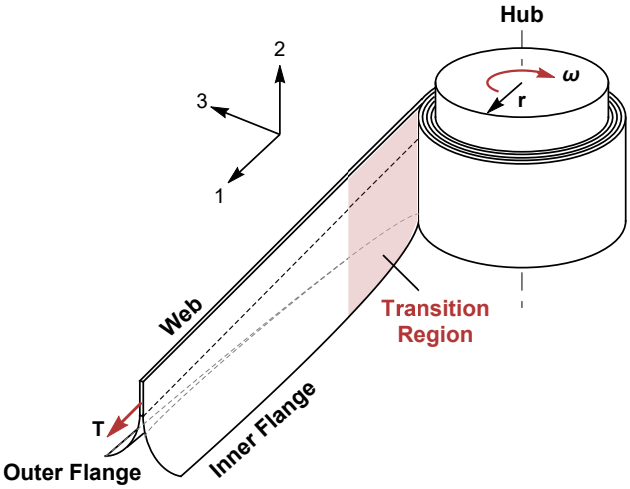

Fig. 2 Schematic of coiling.

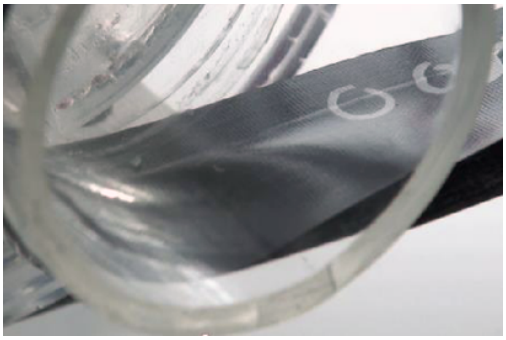

Fig. 3 Propagating buckle in the inner flange.

and experiments indicate that the buckling behavior is sensitive to the flange width. As the physical mechanism underlying the formation and propagation of this buckle still remains unclear, in the current paper we focus on studying the root cause of the buckling and methods to mitigate it.

The specific boom that is analyzed in this paper measures 470 mm in length and has the following cross section dimensions: web width $w = 8$ mm, flange thickness $t = 72\ \mu m$, web thickness $2t + t_b = 144\ \mu m$, flange radius $R = 10$ mm, and $\theta_f = 105°$. The boom consists of a $[0/90]_s$ composite laminate (0° in longitudinal direction). The radius of the coiling hub is 25 mm.

In the present paper, we analyze only the elastic behavior of the propagating buckle, which provides insights for future study of its inelastic behavior. The paper is organized as follows.

We start by presenting a numerical study involving high-fidelity coiling simulations. Following from observations based on the simulation results, we analyze the coiling kinematics. Finally, we discuss the buckling and post-buckling response of the transition region and propose a way to mitigate the buckle magnitude.

II. Numerical Study

A. Finite Element Model

The finite element model to simulate the coiling process is based on the model discussed in [7]. The model is made of a rigid hub and an elastic boom. The boom is modeled as two separate shell structures (tape springs) with nodes tied in the web region. To avoid showing results in the global coordinate system, we define the local material frames 1,2, and 3 for the shell elements. We rely on the local frames shown in Fig. 2 to visualize quantities in the longitudinal and transverse directions of the boom. Axes 1, 2, and 3 represent the longitudinal, transverse, and normal directions respectively. As a consequence, stresses, strains, and curvatures shown in the local frames are corotational quantities that are invariant under the finite rotation during coiling.

The simulation consists of 3 steps: flattening, applying tension, and rolling. First, the root of the two flanges is flattened by the combined flattening pressure $p = 200$ kPa in the bonding region and the upward movement of the hub. At the end of this step, the top and bottom flanges near the root of the boom are flattened, contacting the hub. Second, a 15 N tension is applied at the tip of the boom to straighten it. It guarantees the coiled part will not buckle or detach from the hub. Finally, the root of the boom is rotated around the hub at a prescribed angular velocity of 0.3 rev./s, which allows the boom to coil around the hub. A quasi-static time stepping was carried out with the Dynamic-Implicit module in Abaqus. As for the mesh and element type, S4R elements are used in the model, with 25 elements in the transverse direction.

B. Material Constitutive Relations

The boom is modeled as purely elastic composite shell elements (S4R). The fixed laminate properties are $E_{11} = 128$ GPa, $E_{22} = 6.5$ GPa, and $\nu_{12} = 0.35$. Besides, we consider four different in-plane shear moduli $G_{12} = 3.75$ GPa, 7.5 GPa, 15 GPa, and 30 GPa. The corresponding Q matrices for each ply are:

$$Q_{0^\circ} = \begin{bmatrix} 128.8 & 2.289 & 0 \\ 2.289 & 6.541 & 0 \\ 0 & 0 & G_{12} \end{bmatrix} \text{GPa} \tag{1}$$

and

$$Q_{90^\circ} = \begin{bmatrix} 6.541 & 2.289 & 0 \\ 2.289 & 128.8 & 0 \\ 0 & 0 & G_{12} \end{bmatrix} \text{GPa} \tag{2}$$

where G_{12} takes the four different values mentioned above. Based on the classical lamination theory (CLT), the shell stiffness matrix can be expressed in terms of the ABD matrix, where $A = \sum_k Q_k(z_k - z_{k-1})$, $B = \sum_k Q_k(z_k^2 - z_{k-1}^2)$, and $D = \sum_k Q_k(z_k^3 - z_{k-1}^3)$. For the shell stiffness in the Abaqus model, we use the following ABD matrices obtained from the Q matrices:

$$A = \begin{bmatrix} 4.872 & 0.1648 & 0 \\ 0.1648 & 4.872 & 0 \\ 0 & 0 & (7.2 \times 10^{-5})G_{12} \end{bmatrix} \times 10^6 \; N/m \tag{3}$$

$$B = 0 \tag{4}$$

$$D = \begin{bmatrix} 358.2 & 8.9 & 0 \\ 8.9 & 168 & 0 \\ 0 & 0 & (3.89 \times 10^{-14})G_{12} \end{bmatrix} \times 10^{-5} \; Nm \tag{5}$$

III. High Fidelity Simulation of Buckle Formation

Some qualitative observations regarding the buckling of the boom while coiling around the hub can be made from the numerical simulations. Fig. 4 shows the evolution of transverse curvature change during coiling for the case of $G_{12} = 7.5$ GPa. The inner flange is first locally flattened by the hub (Fig. 4.b). When a critical hub rotation is reached, the inner flange buckles in the transition region (Fig. 4.c). This buckle is unstable and propagates instantaneously until it

reaches the web-flange interface (Fig. 4.d). As coiling continues, the buckle further localizes until a steady state is reached at about a full revolution of the hub (Fig. 4.e). The outer flange does not buckle at all. Its shape remains similar to that of the inner flange in the pre-buckling stage. It is worth noting that the maximum change of transverse curvature is about 0.15 mm^{-1}, which is equivalent to coiling a flat flange around a hub of radius 6.67 mm, about one third smaller than the initial radius of curvature (10 mm) for each flange.

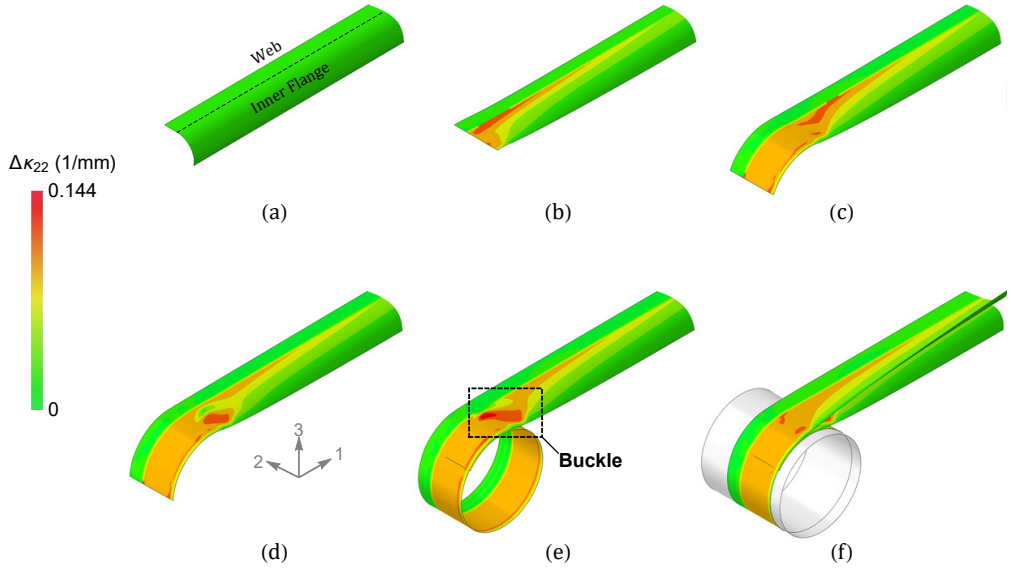

Fig. 4 Evolution of curvature change in transverse direction (G_{12} = 7.5 GPa): (a) Initial configuration of inner flange; (b) Inner flange being flattened and tensioned; (c)-(d) Formation of buckle on the inner flange as the coiling angle increases; (e) The buckle localizes and reaches the steady state; (f) The whole boom at steady state. The views shown in this figure are truncated at the position where flattening and buckling have negligible effects.

When we take a look at the stress contour in the steady state (Fig. 5), we observe that the stress and strain profiles in the coiled region are almost symmetric: the tip and the root of the coiled flange region show much smaller compression but much larger shear than in the middle. Qualitatively, this reminds us of the shear-lag model [8–10], where tension or compression is transmitted through interface shear. After the steady state is reached, only the high compression region of the inner flange (in the middle) keeps getting longer, whereas the two high shear zones at the ends remain stationary. As a result, the stresses become "self-sustained" in the coiled region, transmitting only a fraction of compression to the transition region. The shear-lag theory has been used to model the longitudinal stress distribution in thin shells and

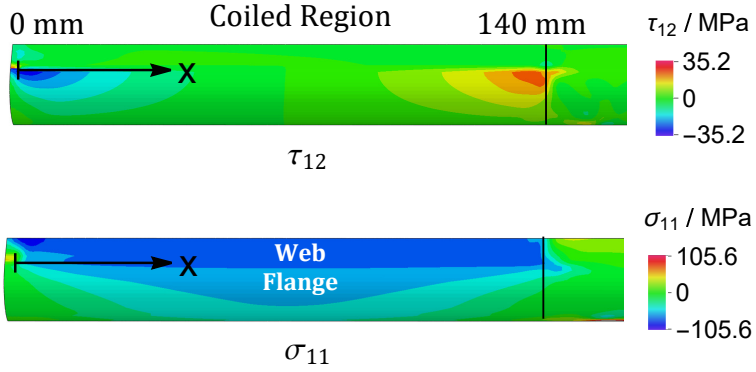

Fig. 5 Shear and compression contours at steady state.

short fibers in composites. An analysis based on the shear-lag theory yields the following fiber stresses:

$$\sigma_f = E_f \varepsilon_1 [1 - \cosh(nx/\rho_f)\mathrm{sech}(ns)] \tag{6}$$

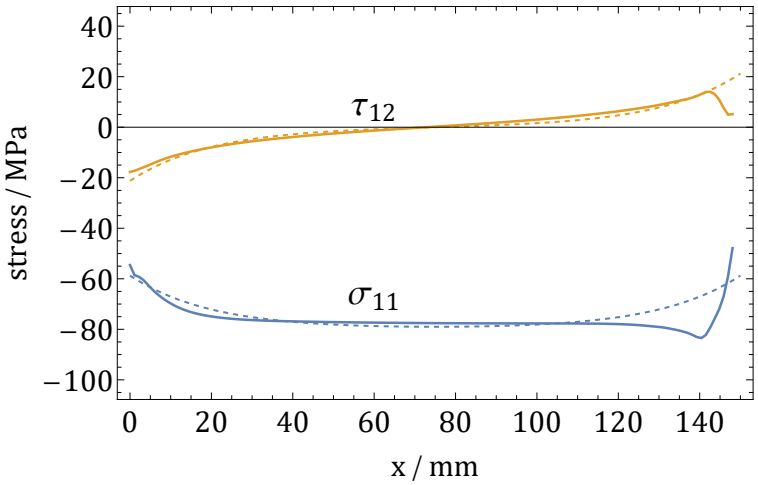

Fig. 6 Shear and compression along the web-flange interface at steady state. Solid curves are stresses obtained from simulations, dashed curves are optimum fit of the simulated curves by the shear-lag model.

and the matrix-fiber interface shear stress follows a hyperbolic sine

$$\tau = \frac{n\varepsilon_1}{2} E_f \sinh(nx/\rho_f)\mathrm{sech}(ns) \tag{7}$$

where ε_1 = overall composite strain, ρ_f = fiber radius, E_f = fiber Young's modulus, and n is a dimensionless constant that depends on fiber and matrix properties. Comparing these two expressions with the stress profile in Fig. 6, both the interface shear and axial compression agree very well with the shear-lag theory. The major discrepancy lies at the right end (x =140 mm) of the coiled region, where the buckle affects the stress distribution, making the simulated stress profile deviate from the shear-lag theory.

Based on the observation that the compression in the coiled flange region is transmitted from the web through the interface shear, it is hypothetical that the shear angle, denoted by γ, directly controls the ultimate magnitude of the buckle. In other words, this coiling instability can be treated as a buckling problem under displacement control, where the shear angle at the coiled-transition region interface is the driving parameter.

IV. Coiling Kinematics - Source of Compression for Buckling

A. Relative slip δ and shear angle γ

In light of the qualitative study in the previous section, it becomes clear that buckling during coiling is directly caused by the compression in the flange section of the transition zone, which is the result of incompatible coiling kinematics of the web and flanges. In this section, we present a detailed discussion of the coiling kinematics of TRAC boom.

Ideally, the boom should coil like a single tape spring, in which case no buckling occurs and the whole boom is under uniform bending stress throughout the structure. Under this perfect coiling scenario, the inner and outer flanges are uniformly compressed and stretched respectively. The neutral surface coincides with the mid-surface of the web. This membrane kinematics accurately reflects what happens in the web section. On the other hand, if the web is missing and the flanges are separate, the mid-surface of each flange will be the neutral surface during coiling. As the result, the two flanges would coil as two separate shells, causing a relative slip between the two flanges. Note that if the ends of the uncoiled region are tied for the two flanges, this relative slip leads to compression of the inner flange and becomes the cause for the buckle. The actual coiling of TRAC boom is intermediate between the two limiting cases discussed above (see Fig 7), where the web tends to coil as a single shell, whereas the flanges want to coil separately. Due to the fact that the web and the flange are connected, high shear stresses develop at the web-flange interface to accommodate this mismatch in kinematics. This allows a portion of the compression at the inner half of the web to leak into the inner flange through the shear-lag mechanism, alleviating the kinematics mismatch. As a result, the slip between the two flanges, δ, is strictly smaller in the actual coiling process compared to the separate coiling scenario. Also different from the coiling

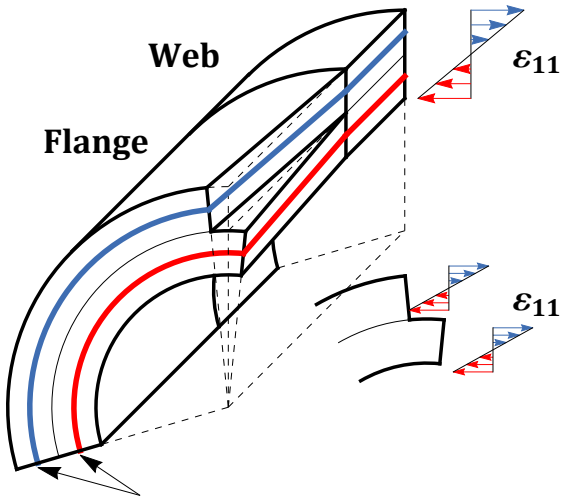

Fig. 7 Schematic showing the coiling kinematics of TRAC booms.

of two separate membranes is that the slip must be 0 at the web-flange interface due to the continuity of displacements. Therefore, a shear angle γ develops at the front of coiled region due to the shear-lag mechanism. It is directly related to the shear stress τ at the interface and the shear modulus G_{12} of the composite. Thus, γ, appears naturally as the work conjugate of the shear stress in the shear-lag region and directly controls the buckling of the transition region.

B. Maximum Slip Allowed by Kinematics: Upper Bound

The maximum possible slip between the inner and outer flanges is determined by the coiling of two separate shells with one on top of the other - free slipping between the two shells. The mid-surface of each flange remains as the neutral surface without any in-plane stretching during the coiling. They keep their original length in the longitudinal direction and the total length of the coiled section for the inner and outer flanges are

$$\left(r + \frac{t}{2}\right)\phi, \text{ and } \left(r + \frac{3t}{2}\right)\phi \tag{8}$$

respectively, where ϕ is the angle of rotation for the hub. It follows that the relative slip between the two flanges, δ, equals their difference:

$$\delta = \phi t \tag{9}$$

Therefore, the maximum possible shear angle is the slip divided by the flange width:

$$\gamma_{\max} = \frac{\delta}{R\theta_f} = \frac{\phi t}{2R\theta_f} \tag{10}$$

This simple expression shows that, in the separate coiling scenario, the relative slip as well as the shear angle between the inner and outer flange grows linearly with the hub rotation. In addition, it is proportional to the flange thickness t as well as the inverse of flange width $1/R\theta_f$.

V. Evolution of γ During Coiling

To understand how the shear angle, γ, evolves, we need to first rigorously define and accurately measure it from the results of the coiling simulation. As this shear angle is at the front of coiled region, which is always above the top of the rotating hub, we need to adopt the Eularian configuration and fix our view at the coiling front. More specifically, we do not define γ based on the material point movement on the hub. Instead, we directly measure the relative slip, δ, of the upper and lower flanges at the coiling front. Then, the shear angle γ is calculated by $\gamma = \delta/R\theta_f$, and we have defined a homogenized shear angle at the coiling front that is measurable. In practice, the relative slip δ at the outer rim of the two flanges are measured via the displacement difference of element nodes that are originally at the same longitudinal position.

The evolution of shear angle γ with the hub rotation is shown in Fig. 8. Despite differences in the shear modulus G_{12}, all of the four curves ($\phi < \pi/2$) start by closely following the upper bound (Eq. 10), indicating that the inner and outer flanges tend to coil separately in the early stage. This is because the compression in the web has not build up yet at the beginning of coiling, and therefore, there is little constraint for the two flanges to coil independently. As the coiling continues and the compression in the inner web section builds up, the shear angle continues to grow, but is gradually slowed down by the compression leak into the coiled inner flange. Therefore, the curves deviate from the separate coiling scenario (the upper bound), and gradually reaches a plateau. During this process, high in-plane axial compression occurs in the transition region of the inner flange, causing its buckling. The buckling events correspond to jumps in the curves near $\phi = \pi/2$.

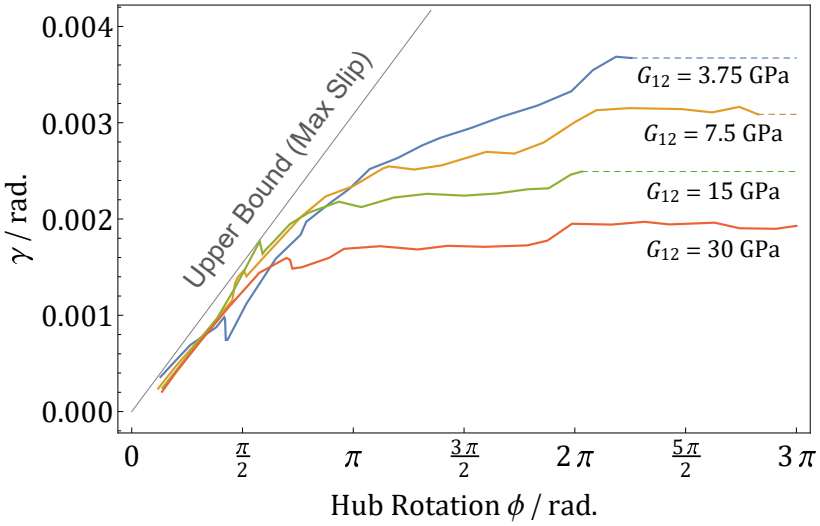

Fig. 8 Evolution of shear angle γ as the hub rotation grows.

One major observation is that the shear modulus has a significant influence on the evolution of γ. The larger the shear modulus, the later the buckling will occur, and the faster the shear angle will stabilize. Most importantly, increasing the shear modulus could substantially reduce the value of γ at the steady state. The shear angle γ further increases a little bit at $\phi = 2\pi$ because the the inner flange starts to coil on top of the outer flange rather than on the hub surface, further increasing the coiling radius. Note that the two simulations with $G_{12} = 3.75$ GPa and 15 GPa terminated relatively early, at around $\phi = 2\pi$, due to contact convergence issues. We have extrapolated the curves using horizontal dashed lines, assuming a steady state is reached.

VI. Buckling and Post-buckling of Transition Region

A. Simplified Buckling Simulation of Transition Region

The shear angle γ, or equivalently the slip, δ, can be seen as the loading parameter for the buckling of the inner flange transition region. In this section, we focus on the buckling response of the transition region under controlled edge shear angle. We use a simple buckling simulation of the transition region using the Abaqus Explicit solver, in which only the inner flange that has not been coiled is modeled (see fig. 9). This is purely a buckling simulation of the

transition region, where we do not consider the coiling process. Nevertheless, the effect of the coiled section on the transition region during coiling is modeled by proper edge loads that produces the similar edge slip δ and shear angle γ. Same as the definition of γ, we adopts the Eularian configuration. In other words, regardless of where the material points move during coiling, we always fix our view in space and model the transition region and the region to be coiled.

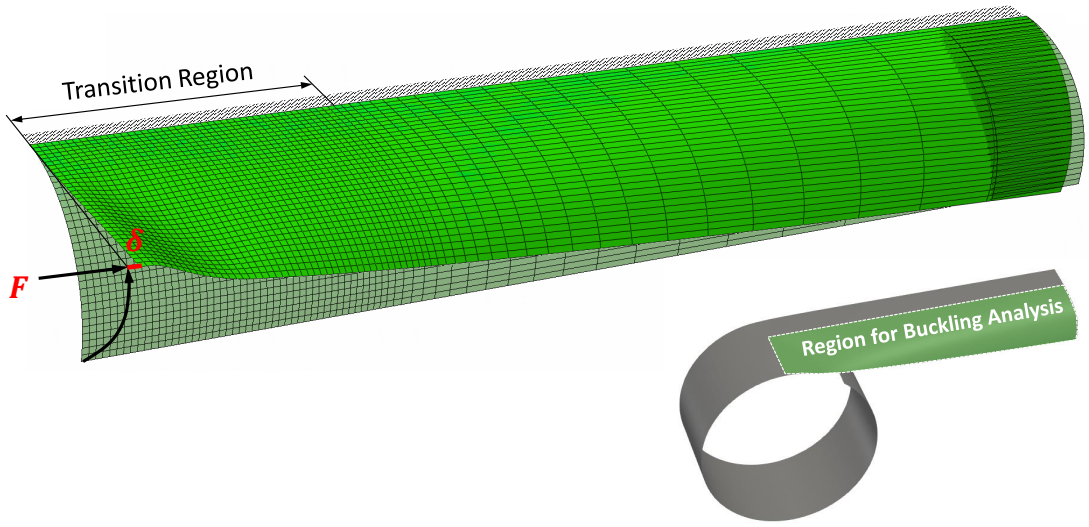

Fig. 9 Schematic of simple buckling simulation. Sub-figure indicates the region of interest.

In this simulation, we only consider the inner half of the original inner flange, using identical material properties and cross section geometry with the coiling simulation. The length of the modeled shell region, L, is chosen as 90 mm. Our main focus, the transition region, is located at the left side of the shell structure being modeled (see Fig. 9). Similar to the coiling simulation, we use the 4-node shell element with reduce integration, S4R. A uniform mesh with element size 0.5 mm is used for the transition region. As the strain gradient is small outside of the transition region, non-uniform course mesh is used to reduce the cost of the computation. As for the boundary conditions, the web is not considered in the model, and is replaced by a clamped boundary condition for simplicity.

In the simulation, we first flatten the left edge of inner flange by controlling the transverse and vertical displacements, u_x and u_y, of the single node at the corner. Next, the shear angle, γ, is produced by prescribing the longitudinal displacement, δ, at the same corner. With the relation between the reaction force F and edge shortening δ, we could understand the buckling and post-buckling behavior of the transition region. Besides, we can qualitatively reproduce the buckle appearing in the high-fidelity coiling simulation.

Despite some differences in loading conditions, this simplified numerical model yields very similar curvature and in-plane strain contours (Fig. 10) compared to the high-fidelity coiling simulation (Fig. 11). It reveals the key features of the buckle initiation and growth for the actual coiling of TRAC booms. From the longitudinal strain contour in Fig. 10, there is a high axial compression region, which we call the compression strut, near the free edge of the transition region prior to the buckling. The buckling is triggered directly by the collapse of this strut. It splits into two smaller compression zones that follow the edges of the buckle. After buckling, the transverse curvature increment gradually grows and concentrates at the web-flange interface. Even though the average in-plane stress values at the mid-surface are below the material strengths, this concentrated curvature could generate very high bending stresses. We believe it is the direct cause of the material damages observed in the TRAC booms [11]. Therefore, in this shear angle controlled buckling process, limiting the magnitude of the in-plane shear deformation at the edge of inner flange is critical to reducing the local material damages during coiling.

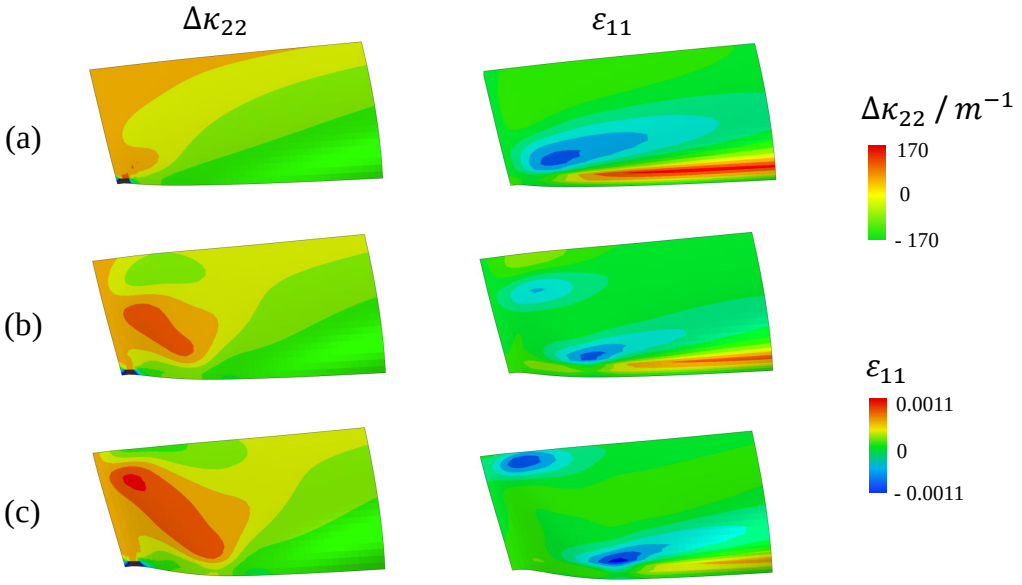

Fig. 10 Evolution of transverse curvature change $\Delta\kappa_{22}$ and in-plane axial compressive strain ε_{11} in the transition region of simplified buckling simulation (G_{12} = 7.5 GPa): a) prior to buckling; b) end of unstable buckle propagation; c) further stable growth of the buckle.

B. Effect of Shear Modulus G_{12}

From the buckling simulation, the measured reaction force F is negative once the flange has been flattened. This indicates that the corner is stretched longitudinally before the buckling. As the change of F relative to the flattened configuration is crucial for the buckling behavior, we show the evolution of the force increment ΔF instead of F. Fig. 11 shows the reaction force-edge shortening relation of the transition region for 4 different material shear moduli G_{12}. From the figure, it is clear that there exists a peak (i.e. buckling strength) for each curve, after which the load immediately drops and gradually rises again. This indicates that the buckling of the transition region undergoes snap-through buckling under load control. It explains why the buckle is initially unstable in the coiling simulation. Thanks to the displacement control in the buckling simulation, we could obtain the post-peak response of the transition region. The drop in reaction force after the peak load is similar to the propagation of instabilities discussed in [12–16], but in our case, the load gradually builds up rather than remaining at a lower level, allowing the buckle to stabilize. The increasing sections of the load-displacement curve after the initial buckling corresponds to the process of buckle growth, where curvatures and stresses build up locally. By comparing the four load-edge shortening curves in Fig. 11, we could clearly see the effect of shear moduli G_{12}. Increasing the shear modulus has two major consequences. It enhances the buckling strength and the in-plane stiffness of the transition region, both of which are beneficial to preventing or mitigating the buckling.

The transverse curvature change, $\Delta\kappa_{22}$, is a good indicator of the buckling magnitude. It is also the most critical variable for material damage as it is the curvature change induced by both flattening and buckling. Fig. 12 shows the effect of the laminate shear modulus G_{12} on the spatial distribution of $\Delta\kappa_{22}$ near the coiling buckle at about one hub revolution. As G_{12} increases gradually from 3.75 GPa to 30 GPa, the area of the high curvature contour decreases dramatically. Also decreases is the maximum curvature $\Delta\kappa_{22_{\max}}$: from 143 m^{-1} at G_{12} = 3.75 GPa to 132.8 m^{-1} at G_{12} = 30 GPa. Since the radius of the flange is 10 mm, the transverse curvature increase due to flattening alone is 100 m^{-1}. Therefore, the amount purely induced by buckling decreased from 43 m^{-1} to 32.8 m^{-1}, which is drop of about 25%. It suggests that increasing the shear modulus, G_{12}, of the laminate does mitigate the buckling magnitude, and hence could be useful for preventing material damage during coiling.

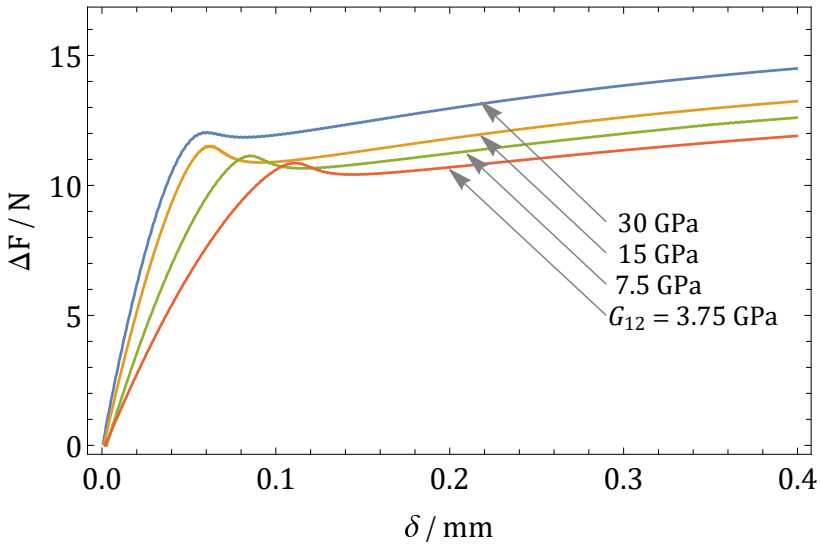

Fig. 11 Edge load-shortening curve for the composite shell.

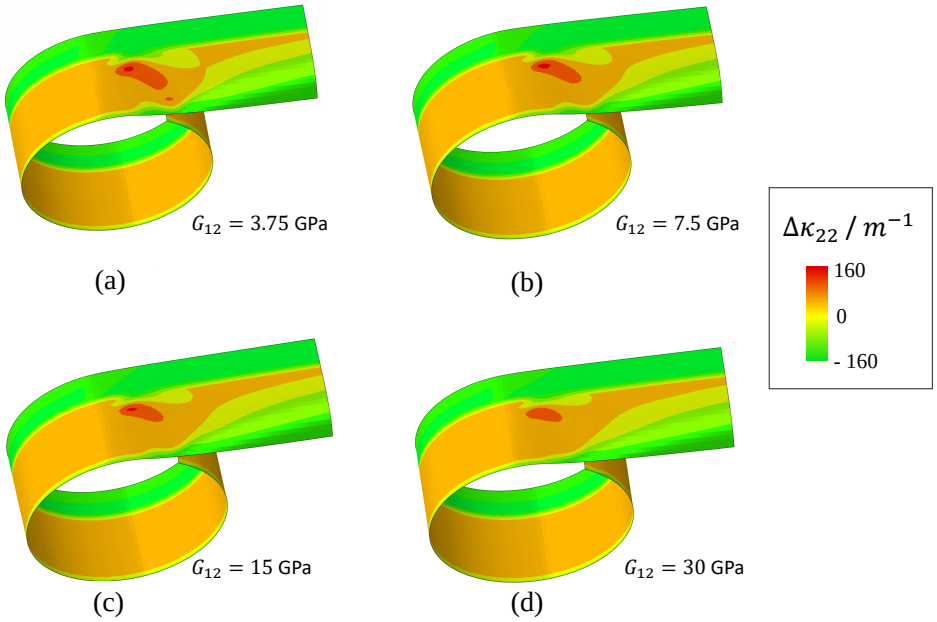

Fig. 12 Effect of G_{12} on the transverse curvature change $\Delta\kappa_{22}$ during coiling.

VII. Conclusions and Discussion

In the current study, we have discussed the underlying mechanism for the coiling instability of composite TRAC booms. The main conclusions are summarized in the following:

1) The buckling of composite TRAC booms during coiling originates from their geometry. It occurs as a result of the coiling kinematic mismatch between their free and seamed edges.
2) The in-plane deformation of the web and the inner flange is coupled through shear-lag mechanism. It helps mitigate but does not completely eliminate their coiling kinematics mismatch, leading to the formation of a compression strut in the transition region.
3) The buckling belongs to the class of snap-through instability. It is directly caused by the collapse of an effective "compression strut" in the transition region.
4) The buckle does not grow forever. After a sufficient length has been coiled, the structure always reaches a steady

state in the simulation, where the maximum concentrated curvatures are observed. In practice, local material damage could occur to release the stress/curvature concentration. As the coiling continues after the cracking, another cycle begins where the stress and curvature build up again until the energy is released by the next fracturing event, leading to quasi-periodic distributed cracks and delaminations along the length of the boom.

5) To mitigate the size of the buckle and avoid local material failures during coiling, the key is to limit the growth of the shear angle γ from the shear-lag mechanism. The current study explores the possibility of increasing the in-plane shear modulus, G_{12}, of the composite to achieve this goal. Simulations show that this method is beneficial to curbing the growth of the buckle. Unlike isotropic materials, orthotropic materials such as carbon fiber reinforced polymers (CFRP), do have a wide range of G_{12}/E_{11}. Therefore, increasing the in-plane shear modulus of each ply is a feasible direction for booms made from composite materials to limit the growth of the coiling buckle.

References

[1] Miura, K., and Pellegrino, S., *Forms and Concepts for Lightweight Structures*, Cambridge University Press, 2020.

[2] Banik, J., and Murphey, T., "Performance validation of the triangular rollable and collapsible mast," 2010.

[3] Seffen, K., and Pellegrino, S., "Deployment dynamics of tape springs," *Proceedings of the Royal Society of London. Series A: Mathematical, Physical and Engineering Sciences*, Vol. 455, No. 1983, 1999, pp. 1003–1048.

[4] Hoskin, A., Viquerat, A., and Aglietti, G. S., "Tip force during blossoming of coiled deployable booms," *International Journal of Solids and Structures*, Vol. 118, 2017, pp. 58–69.

[5] Wang, S., Schenk, M., Jiang, S., and Viquerat, A., "Blossoming analysis of composite deployable booms," *Thin-Walled Structures*, Vol. 157, 2020, p. 107098.

[6] Cox, K., and Medina, K., "An Investigation of Inner Flange Buckling in Furlable Composite Booms," *Proceedings of the American Society for Composites—Thirty-third Technical Conference*, 2018.

[7] Leclerc, C., "Mechanics of Ultra-Thin Composite Coilable Structures," Ph.D. thesis, California Institute of Technology, 2020.

[8] Clyne, T. W., and Hull, D., *An introduction to composite materials*, Cambridge University Press, 2019.

[9] Fan, H.-T., "A study of" shear lag" phenomenon in a stiffened flat panel by photoelastic methods," Ph.D. thesis, California Institute of Technology, 1939.

[10] Sørensen, R., "Evaluation of shear lag in standard H-/I-sections," *Aalborg University Esbjerg, Denmark*, 2013.

[11] Hasanyan, A. D., Leclerc, C., and Pellegrino, S., "Interface Failure Analysis of Triangular Rollable and Collapsible (TRAC) Booms," *AIAA Scitech 2020 Forum*, 2020, p. 0694.

[12] Chater, E., and Hutchinson, J., "On the propagation of bulges and buckles," *ASME. Journal of Applied Mechanics.*, 1984.

[13] Chater, E., and Hutchinson, J., "Mechanical analogs of coexistent phases," *Phase Transformations and Material Instabilities in Solids*, 1984, pp. 21–36.

[14] Kyriakides, S., "Buckle propagation in pipe-in-pipe systems.: Part I. Experiments," *International Journal of Solids and Structures*, Vol. 39, No. 2, 2002, pp. 351–366.

[15] Shaw, J. A., and Kyriakides, S., "Initiation and propagation of localized deformation in elasto-plastic strips under uniaxial tension," *International journal of plasticity*, Vol. 13, No. 10, 1997, pp. 837–871.

[16] Li, Z., and Sun, Q., "The initiation and growth of macroscopic martensite band in nano-grained NiTi microtube under tension," *International Journal of plasticity*, Vol. 18, No. 11, 2002, pp. 1481–1498.